Supplemental Material

Experimental Design:

Male C57BL/6J mice (10-15 weeks old) were purchased from the Jackson Laboratory (Bar Harbor, ME) and were acclimatized for 5 days prior to any study procedures. All animals (n=78) were housed in a temperature-controlled facility (22-24 C°), kept on a 12:12 hour light:dark cycle, and fed a standard chow diet *ad libitum* for the duration of the study. All animals were used in accordance with protocols and policies approved by the Yale Institutional Animal Care and Use Committee. Animals were separated into two groups that allowed for a) *in vivo* specificity of hNIS-mediated $^{99m}TcO_4^-$ uptake (n = 42), and b) serial assessment of hNIS expression over 28 days (n = 36) as illustrated in Figure 1.

Forty-two animals were included in the blocking study. Of these, 24 animals underwent unilateral HLI (right leg). Seven days following surgery, the ischemic GA muscle was injected with AAV9-hNIS with (n=12) or without NA (n=12) as described below. The contralateral limb was injected with PBS (n=18) or remained without injection (n=6). Twelve mice were injected with AAV9-hNIS + NA in the right GA and AAV9-hNIS alone in the left GA. An additional 6 mice served as vehicle controls, in which the right GA was injected with PBS, while the left GA remained untreated. On day 10 following injection, these animals underwent microSPECT/CT imaging following administration of $^{99m}TcO_4^-$ alone or co-injected with the widely used NIS competitive inhibitor perchlorate (ClO_4^-) [1, 2], to ascertain the specificity of $^{99m}TcO_4$ uptake. Following imaging, animals were euthanized and tissue was harvested for well counting and biochemical assays. Note, at this timepoint a larger tissue volume was allocated for western blot analyses. A schematic representation of the blocking group study design is illustrated in Figure 1A.

Thirty-six animals were included in the time course study. Of these, 24 animals underwent unilateral HLI (right leg). Seven days following surgery, the ischemic gastrocnemius (GA) muscle was injected with AAV9-hNIS with (n = 12) or without NA (n = 12), while the contralateral limb was injected with PBS. The remaining mice (n = 12) were injected with AAV9-hNIS + NA in the right GA and AAV9-hNIS alone in the left GA. Of these, 12 mice underwent serial microSPECT/CT imaging after administration of $^{99m}TcO_4^-$ on day 3, 7, 10, 14 and 28 following injection of AAV9-hNIS. Following imaging on day 28, animals were euthanized and tissue was harvested for well counting and biochemical assays. At this later timepoint, a larger volume of tissue was allocated for well counting. In addition to the animals that were imaged, a subgroup of mice (n=4 per group) for each of the five treatment arms were euthanized on day 3 and 14 following $^{99m}TcO_4^-$ injection to validate time-dependent changes in image-derived $^{99m}TcO_4^-$ uptake with well counting and hNIS protein expression with western blot analysis. A schematic representation of the time-course study is illustrated in Figure 1B.

Animal Procedures:

Unilateral Hind-limb Ischemia Surgery

Forty-eight mice underwent surgical occlusion of the right femoral artery to induce unilateral HLI according to the procedure described in detail elsewhere [3-5]. Briefly, animals were anesthetized with 2% isoflurane and maintained at constant temperature (37°C) for the duration of the surgery. The skin overlying the right femoral artery was shaved and sterilely prepped prior to exposing and isolating the right femoral artery. Following isolation of the femoral artery, two ligatures (6.0 silk) were placed distal to the profundus branch (~1 mm apart) and this segment was transected in between the ligatures to create HLI. Notably, this ligation site induces ischemia

in musculature of distal hind-limb, particularity in the distal hamstring, gastrocnemius (GA) and soleus muscles [5].

AAV9 vector and Neuraminidase delivery

The AAV9 vector system used incorporates a cytomegalovirus (CMV) promoter driving the expression of hNIS linked to eGFP via an IRES element (AAV9 pzac2.1-CMV-NIS-IRES-eGFP [AAV9-hNIS], ViGene Biosciences, Rockville, MD) and was delivered intramuscularly ($2*10^{11}$ viral genome particles [vgp]) into the GA muscle with a 31-gauge insulin needle as described in the supplemental methods. For all injections, mice were anesthetized with 2 % isoflurane and the hair overlying the GA muscle was removed (Nair, Church & Dwight) to assist in the visualization of the underlying anatomy. AAV9-hNIS was then delivered as two separate longitudinal injections into the lateral and medial heads of the GA (two 20 μL injections totaling $2*10^{11}$ viral genome particles [vgp]) of both ischemic and non-ischemic muscle. In addition, in a subgroup of mice, NA from *Vibrio cholera* type II (0.010 units) was mixed with AAV9-hNIS ($2*10^{11}$ vpg) and injected into ischemic or non-ischemic muscle. Also, as described above, controls limbs were injected in an identical fashion to vector injections with a matched volume of PBS (40 μL). In pilot experiments, a viral load of $2x10^{11}$ vpg was the lowest dose that enabled reproducible detection of $^{99m}TcO_4^-$ uptake on microSPECT imaging in the AAV9-hNIS alone group, which represented our lowest expression group; therefore, this dose was chosen for all subsequent experiments.

MicroSPECT/CT Image Reconstruction

List mode data were reconstructed using the photopeak of ^{99m}Tc (126 - 154 keV) along with background windows below (120.4 - 126 keV) and above (154.0 - 159.6 keV) the photopeak. SPECT images were reconstructed by means of ordered subset expectation

maximization (OS-EM) with 8 subsets and 9 (time course group) or 25 iterations (blocking group) using system software (MILabs-Rec, version V3.26). These algorithms yielded a 65*70*268 image size with a voxel size of 0.4*0.4*0.4 mm^3. CT images were reconstructed using the filtered back-projection algorithm with a Hann projection filter that generated a 0.8x0.8x0.8 mm^3 voxel size and 288*241*1528 voxel number. Finally, SPECT images were registered to CT images using system software. All SPECT images were decay-corrected and reconstructed voxel values expressed as mCi/cc, using a previously determined calibration factor.

MicroSPECT/CT Image Analysis

We trained a deep neural network to perform segmentation of the volumes of interest (VOIs) of the left and right GA muscles on microCT images (Figure 2, public GitHub repository https://github.com/j-onofrey/deepimage-legacy).We adopted a modified version of the U-Net[6] fully-convolutional encoding-decoding architecture. Our implementation of this network differed from the standard U-Net architecture in that we used three max-pooling operations (instead of the standard four) and reduced the number of convolution kernels by half. We used a patch-based training and segmentation approach, using image patches of size 32x32x32 voxels. For training, we extracted mini-batches of size 32 by uniform random sampling overlapping patches from the training data set of manually segmented VOIs of the left and right GA using in-house software (version 0.9.10, BioImage Suite, Yale University, New Haven, CT). To augment our training set, we randomly flip patches left and right to take advantage of anatomical symmetries. We train the model by optimizing the cross-entropy loss function using the Adam optimizer with learning rate 0.0001. First, we trained the model for a total of 4,096 iterations. We then re-trained the model a

second time for another 2,048 iterations, but added a regularization term to the loss function to enforce smoothness in the segmentation results.

To segment a test image not included in the training set, we uniformly sample overlapping patches from the test image at increments of half the patch size in each dimension. Once all patches have been segmented from the image volume, we reconstruct the whole image field of view's segmentation by performing a weighted combination of the segmented patches. Here, the voxel segmentation results are weighted according to their distance from the patch center, and we threshold the segmentation results at 0.5. We implemented the model using TensorFlow and ran all computations on an NVIDIA GTX 1080 Ti GPU with 11 GB RAM.

Finally, we performed a cluster thresholding of the resulting segmentation to identify the two VOIs, and then applied a 3D median filter to remove any spurious artifacts from the segmentation results.

$^{99m}TcO_4^-$ retention on microSPECT images was then quantified by applying the generated VOIs onto the microSPECT images, which were previously registered to microCT images, to derive mean image count activity in mCi/cc using BioImage Suite, as previously described [4, 7]. Image activity in mCi/cc was then corrected by injected dose and animal body weight in grams (g) and displayed as SUV for image quantification.

In order to appropriately visualize the spatial-temporal change in gene expression over time, representative serial SPECT/CT images were semi-automatically registered using algorithms available in BioImage Suite, as previously described [8]. Briefly, using the CT on day 3 as a reference, each subsequent CT from each time point was non-rigidly registered to this reference CT by using an algorithm that used the normalized mutual information as the similarity metric. Since each CT image was previously registered with each corresponding SPECT image, the

transformation matrices derived above were applied to the corresponding SPECT images. Displayed representative SPECT/CT were created using AMIDE software (version 1.0.4) [9], with the display scale for each image being normalized to injected dose and body weight and was expressed as SUV.

Immunoblotting

GA muscles (~0.25 g) were placed in 2 mL of homogenization buffer (20 mM HEPES, pH 7.4; 250 mM Sucrose; 2 mM EDTA; 1:500 Protease Inhibitor Cocktail, Roche) and homogenized on ice with a bench top homogenizer (Brinkmann Polytron P20 Generator). The homogenate was centrifuged at 1,300 × g for 10 min (Beckman JA-20.1, 3.5K rpm). The resulting supernatant was centrifuged at 229,000 × g for 60 min (Beckman 70.1 Ti, 50K rpm) to isolate the total membrane fraction. The total membrane fraction was then solubilized in 20 mM HEPES, pH 7.5; 137 mM NaCl; 1 % (v/v) Nonidet P-40; 10% glycerol; 1 mM EDTA and 1:500 Protease Inhibitor Cocktail (Roche). The protein content of the total membrane fraction was determined by using the BCA Protein Assay (Thermo Fisher Scientific, Waltham, MA). Membrane proteins (20 µg) were resolved by SDS-PAGE and blots probed with 4nM affinity-purified anti-human NIS antibody followed by anti-rabbit secondary antibodies (1:3,000; Jackson ImmunoResearch Laboratories, West Grove, PA). Proteins were visualized using Super-Signal PICO Plus Chemiluminescent Substrate (ThermoFisher).

Membrane proteins (20 µg) were resolved by SDS-PAGE and blots probed with 4nM affinity-purified anti-human NIS antibody followed by anti-rabbit HRP-conjugated secondary antibody (1:3,000; Jackson ImmunoResearch Laboratories, West Grove, PA). Proteins were visualized using Super-Signal West Pico PLUS Chemiluminescent Substrate (ThermoFischer). Total protein loaded was evaluated by Coomassie blue staining of the blotted membrane. Band

intensities were measured densitometrically using ImageJ software (version 1.6.0_24, U.S. National Institutes of Health, Bethesda, MD, USA) and quantitated against total protein.

Immunofluorescence

After fixation in 10% buffered formalin for 24-48 hours, skeletal muscle tissue was paraffin-embedded and cut into 3-5 μm sections. To determine NIS expression, tissue slices were deparaffinized, rehydrated, and permeabilized for 1 hr at 4^0C using a PBS-based blocking buffer (pH 7.4) containing 50 mM glycine, 5% goat serum, 2.5% BSA, 0.05% sodium azide, and 0.03% saponin. Samples were then incubated overnight at 4^0C with primary antibodies (hNIS, 1:1000) in PBS-based incubation buffer (FIB; pH 7.4) containing 50 mM glycine, 1% goat serum, 0.25% BSA, 0.05% sodium azide, and 0.03% saponin. Slides were washed 3 x 20 min with PBS, fixed in 1% paraformaldehyde (5 min), washed in PBS, and quenched with 0.125 M glycine (10 min). Tissues were incubated in FIB with anti-rabbit secondary antibodies Alexa 595-conjugated (2 hr in the dark at 4^0C), in PBS, and coverslips were mounted on glass slides with fluorescence mounting medium (Vectashield, Vector). NIS expression was visualized by fluorescence microscopy using a Zeiss LSM 800 Airyscan confocal microscope. In addition, eGFP expression was also visualized to co-validate AAV9-mediated gene expression and distribution, as the AAV9 vector also expressed eGFP.

Supplemental Figure 1

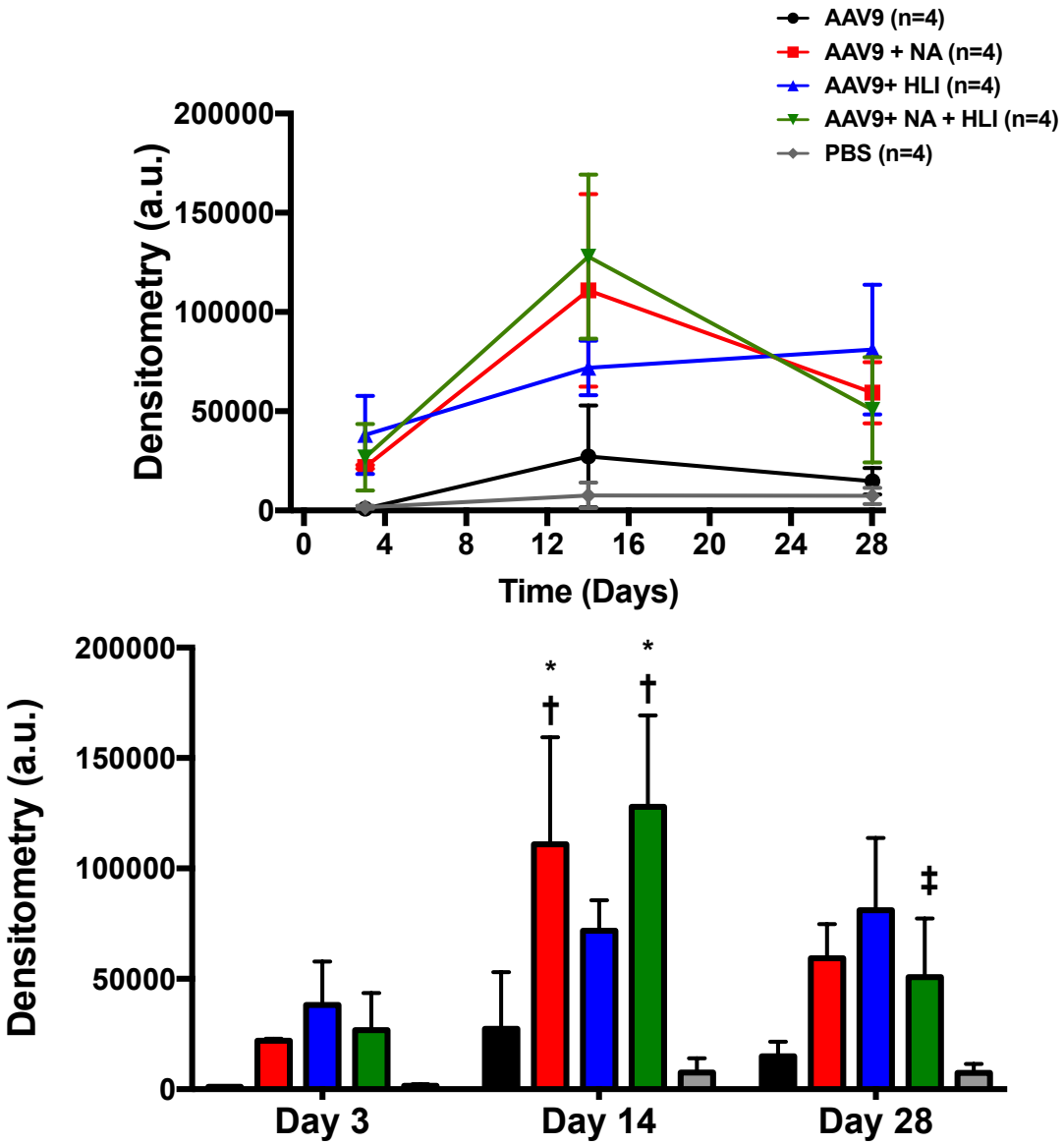

Supplemental Figure 2

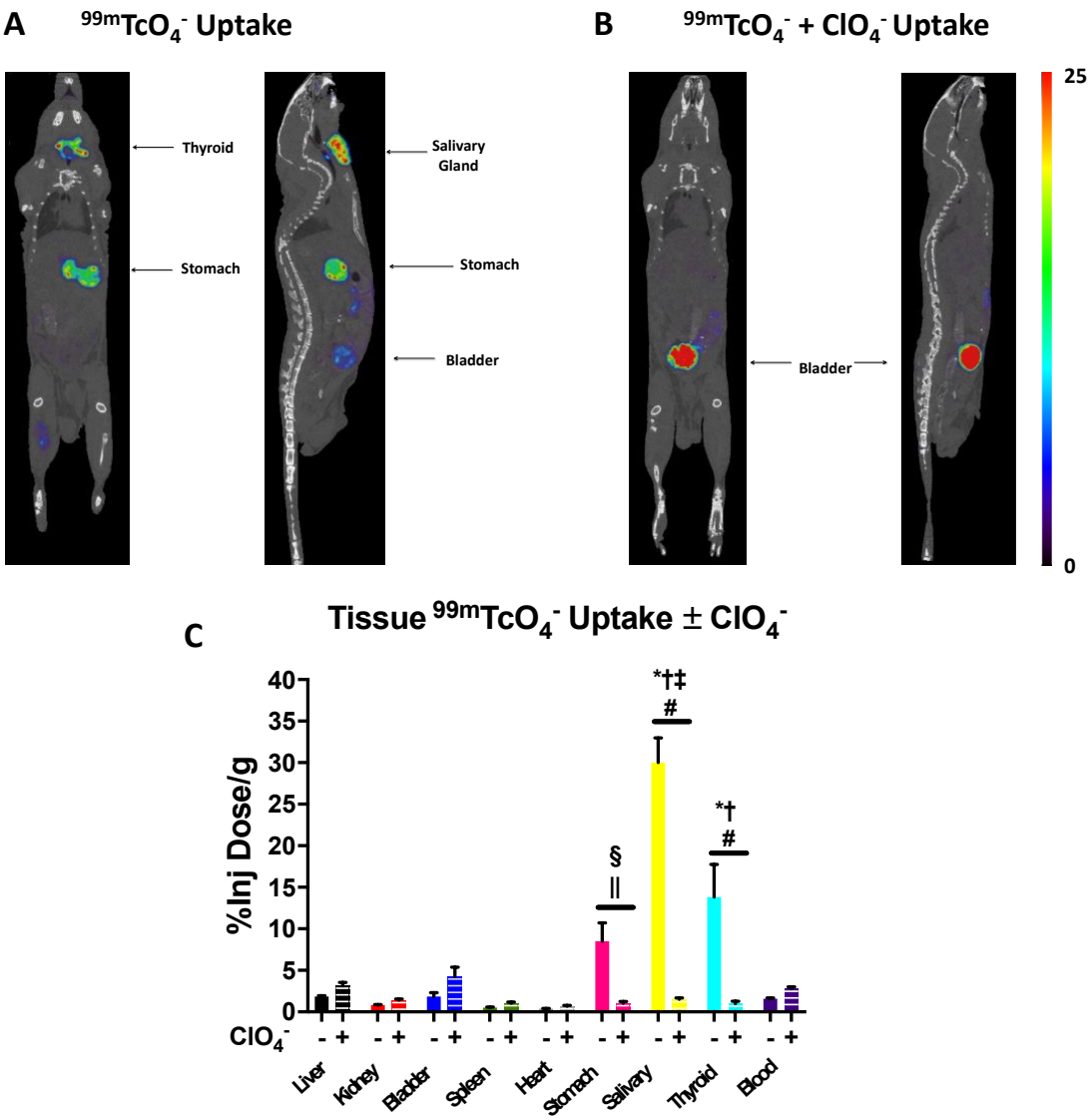

Supplemental Figure Legends

Supplemental Figure 1: *AAV9-mediated NIS expression increases over time.* **A)** Time course and **B)** quantitative determination of NIS expression over time by immunoblot. * = P<0.05 vs. PBS; † P<0.05, and ‡ = P<0.05 vs. Day 28. AAV9= adeno-associated virus 9, A.U.= arbitrary units, HLI= Hind-limb ischemia, NA= neuraminidase, PBS= phosphate-buffered saline, SUV= standardized uptake value.

Supplemental Figure 2: *ClO_4^- inhibits $^{99m}TcO_4^-$ uptake in NIS-expressing tissues.* **A)** Representative coronal and sagittal microSPECT/CT images of whole-body $^{99m}TcO_4^-$ uptake on day 10 following AAV9-hNIS injection in a mouse co-treated with neuraminidase and AAV9-hNIS. **B)** Same as A, except that $^{99m}TcO_4^-$ was co-administered with ClO_4^-. Image quantification and display is the same as in Figure 3. For gamma well counting, $^{99m}TcO_4^-$ tissue activity is expressed as % injected dose per gram of tissue. * P < 0.0001 vs. all non-NIS-expressing tissues (liver, kidney, bladder, spleen, heart, and blood); †= P < 0.0001 vs. stomach, ‡= P< 0.0001 vs. thyroid and §= P<0.0001 vs. heart, but no other non-NIS-expressing tissues. || =P<0.001 within group difference between mean $^{99m}TcO_4^-$ tissue uptake with and without ClO_4^-; # =P<0.0001 within group difference between mean$^{99m}TcO_4^-$ tissue uptake with and without ClO_4^-. Inj.= Injected, g=gram.

References:

1. Tazebay UH, Wapnir IL, Levy O, Dohan O, Zuckier LS, Zhao QH, Deng HF, Amenta PS, Fineberg S, Pestell RG. The mammary gland iodide transporter is expressed during lactation and in breast cancer. *Nature medicine*. 2000;6:871
2. Dohán O, Carrasco N. Advances in na+/i− symporter (nis) research in the thyroid and beyond. *Molecular and cellular endocrinology*. 2003;213:59-70
3. Hua J, Dobrucki LW, Sadeghi MM, Zhang J, Bourke BN, Cavaliere P, Song J, Chow C, Jahanshad N, van Royen N. Noninvasive imaging of angiogenesis with a 99m tc-labeled peptide targeted at α v β 3 integrin after murine hindlimb ischemia. *Circulation*. 2005;111:3255-3260
4. Dobrucki LW, Dione D, Kalinowski L, Dione D, Mendizabal M, Yu J, Papademetris X, Sessa WC, Sinusas AJ. Serial non-invasive targeted imaging of peripheral angiogenesis: Validation and application of a semi-automated quantitative approach. *Journal of nuclear medicine: official publication, Society of Nuclear Medicine*. 2009;50:1356
5. Hedhli J, Slania SL, Płoska A, Czerwinski A, Konopka CJ, Wozniak M, Banach M, Dobrucki IT, Kalinowski L, Dobrucki LW. Evaluation of a dimeric-crgd peptide for targeted pet-ct imaging of peripheral angiogenesis in diabetic mice. *Scientific reports*. 2018;8:5401
6. Ronneberger O, Fischer P, Brox T. U-net: Convolutional networks for biomedical image segmentation. *International Conference on Medical Image Computing and Computer-Assisted Intervention*. 2015:234-241
7. Suh JW, Scheinost D, Dione DP, Dobrucki LW, Sinusas AJ, Papademetris X. A non-rigid registration method for serial lower extremity hybrid spect/ct imaging. *Medical image analysis*. 2011;15:96-111
8. Joshi A, Scheinost D, Okuda H, Belhachemi D, Murphy I, Staib LH, Papademetris X. Unified framework for development, deployment and robust testing of neuroimaging algorithms. *Neuroinformatics*. 2011;9:69-84
9. Loening AM, Gambhir SS. Amide: A free software tool for multimodality medical image analysis. *Molecular Imaging*. 2003;2:15353500200303133